For the LW approximation, usually utilized in correction of Bragg intensities, it must be expected that its results will be worse than those of LWD. The LW approximation tends to increase the frequency mode values with respect to the real ones when we come out of the long-wave limit and this effect will be more important when calculating the background contribution, where the LW approximation is less valid, and therefore the tendency will be an overestimation of the net intensity calculated for the scanned volume with respect to LWD values, similar to the first-order case (Kroon & Vos, 1979).

We thank the Computing Centre of the University of Seville for facilities given to run these rather lengthy calculations and the Spanish Government, which has supported in part this work through the Comisión Asesora de Investigación Científica y Técnica.

References

BORN, M. & HUANG, K. (1968). *Dynamical Theory of Crystal Lattices.* Oxford: Clarendon.
COCHRAN, W. (1963). *Rep. Prog. Phys.* **26**, 1-45.
CRIADO, A., CONDE, A. & MÁRQUEZ, R. (1984) *Acta Cryst.* A**40**, 696-701.
CRIADO, A., CONDE, A. & MÁRQUEZ, R. (1985). *Acta Cryst.* A**41**, 158-163.
HELMHOLDT, R. B., BRAAM, A. W. M. & VOS, A. (1983). *Acta Cryst.* A**39**, 90-94.
HELMHOLDT, R. B. & VOS, A. (1977). *Acta Cryst.* A**33**, 38-45.
KROON, P. A. & VOS, A. (1978). *Acta Cryst.* A**34**, 823-824.
KROON, P. A. & VOS, A. (1979). *Acta Cryst.* A**35**, 675-684.
MARADUDIN, A. A., MONTROLL, E. W., WEISS, G. H. & IPATOVA, I. P. (1971). *Theory of Lattice Dynamics in the Harmonic Approximation.* New York: Academic Press.
PAWLEY, G. S. (1969). *Acta Cryst.* A**25**, 702-707.
RAMACHANDRAN, G. N. & WOOSTER, W. A. (1951). *Acta Cryst.* **4**, 335-344.
STEVENS, E. D. (1974). *Acta Cryst.* A**30**, 184-189.
WALKER, C. B. & CHIPMAN, D. R. (1970). *Acta Cryst.* A**26**, 447-455.

Acta Cryst. (1985). A**41**, 320-327

Interpretation of Dynamical Diffuse Scattering of Fast Electrons in Rutile

BY C. J. ROSSOUW

CSIRO Division of Chemical Physics, PO Box 160, *Clayton* 3168, *Australia*

AND L. A. BURSILL

School of Physics, University of Melbourne, Parkville 3052, *Australia*

(*Received* 15 *September* 1983; *accepted* 4 *December* 1984)

Abstract

An Einstein model for thermal diffuse scattering is extended to a fully dynamical *n*-beam Bloch-wave treatment, where explicit account is taken of the scattering site symmetry from individual atoms. Dynamical effects in this model are related to orientation-dependent fluctuations in current density on localized scattering centres within the crystal, yielding excess or deficit Kikuchi bands. Calculated diffuse scattering distributions are compared with experimental observations from rutile (TiO_2). The predicted diffuse distribution for scattering from oxygen sites correlates reasonably well with experiment, implying a relatively weak contribution for (localized) thermal diffuse scattering of fast electrons from titanium sites.

1. Introduction

The Einstein model for thermal diffuse scattering (TDS) lends itself to interpretation in terms of localized scattering centres within a unit cell. It has been shown that, for ionization events, a Bloch-wave formulation in describing the passage of a fast electron through a crystal can clearly predict the formation of excess or deficient bands in the inelastic beam, depending on (1) diffraction conditions for the elastic and inelastic beams, (2) scattering kinematics and (3) site of interaction within the crystal (Maslen & Rossouw, 1984; Rossouw & Maslen, 1984). In this paper we extend the Einstein model for TDS, developed by Hall & Hirsch (1965), to evaluate the scattering kinematics term in a dynamical *n*-beam Bloch-wave formulation. Computer simulations based on this theory are compared with the diffuse scattering observed from TiO_2 viewed down the *c* axis.

2. Theory

Hall & Hirsch (1965) derived a formula for the TDS intensity as a function of momentum transfer $\hbar\mathbf{q}$ to the crystal, using an Einstein model for uncorrelated thermal displacements of crystal atoms (here $\mathbf{q} = \mathbf{k} - \mathbf{k}'$, where $\mathbf{k}$ and $\mathbf{k}'$ are the wavevectors of the fast

0108-7673/85/040320-08$01.50

electron before and after inelastic scattering). We rewrite the equations in terms of localized scattering sources, extending the Hall & Hirsch model (scattering of a two-beam incident state to an outgoing plane wave) to a fully dynamical n-beam model. A Bloch-wave model is used to describe the incident and scattered fast-electron wavefunctions, $\psi(\mathbf{k})$ and $\psi'(\mathbf{k}')$, based on quantum mechanical theory as developed by Yoshioka (1957), Howie (1963) and Rez, Humphreys & Whelan (1977) amongst others. The appropriate expression that gives the inelastic intensity as a function of $\mathbf{q}$ has been developed by Rossouw & Maslen (1984) for ionization. This is conveniently factorized into summations over terms that depend separately on ψ and ψ' $[k, k']$, site of interaction [site] and appropriate scattering kinematics [kin]. Thus

$$\frac{\mathrm{d}I}{\mathrm{d}\Omega} = nt \sum_{ghg'h'} [\text{site}][\text{kin}] \sum_{iji'j'} [k, k'], \qquad (1)$$

where n is the number of lattice sites per unit volume and t the specimen thickness. The indices (g, h) refer to diffracted beams in ψ, and the primes on (g', h') refer to ψ'. Likewise, primes on the branch indices (i, j) indicate the inelastic state. The term $[k, k']$ is given by

$$[k, k'] = A^{i*}A^{j}A^{i'*}A^{j'}C^{i*}_{g}C^{j}_{h}C^{i'*}_{g'}C^{j'}_{h'}X,$$

where

$$X = \frac{\exp[i(\gamma^{j}-\gamma^{i})t]-\exp[i(\gamma^{i'}-\gamma^{j'})t]}{it(\gamma^{j}-\gamma^{i}-\gamma^{i'}+\gamma^{j'})} \qquad (2)$$

and A^{i} $(=C^{i*}_{0})$ is the amplitude of the Bloch wave on branch i of the dispersion surface, and the C's and γ's are the eigenvectors and eigenvalues of the scattering matrix (see Humphreys, 1979, for a review of the Bloch-wave scattering model).

Defining $\mathbf{Q}_1 = \mathbf{q}+\mathbf{h}-\mathbf{g}'$, $\mathbf{Q}_2 = \mathbf{q}+\mathbf{g}-\mathbf{h}'$, the [site] term is given by

$$[\text{site}] = \sum_{\alpha}\sum_{m} \exp[i(\mathbf{Q}_1-\mathbf{Q}_2)\cdot\boldsymbol{\tau}_{\alpha m}], \qquad (3)$$

where $\boldsymbol{\tau}_{\alpha m}$ is the position vector of the mth atom of type α in the unit cell.

Equations (1)–(3) summarize the general result for localized inelastic scattering sources within the unit cell. This takes into account amplitude summation for inelastic scattering from all diffracted beams *via* $\mathbf{Q}_{1,2}$. The [kin] term now needs to be written as a function of $\mathbf{Q}_1$ and $\mathbf{Q}_2$ from the Einstein TDS model. As for ionization, it is necessary to consider 'non-aligned' terms where $\mathbf{Q}_1 \neq \mathbf{Q}_2$. The Hall & Hirsch result is restricted to a two-beam elastic wavefunction scattering to a plane wave, so that the only 'non-aligned' terms include $\mathbf{q}$ and $\mathbf{q}-\mathbf{g}$. Their expression may be rewritten in terms of (1), with a general [kin] term

$$[\text{kin}] = f_{\alpha}(Q_1)f^{*}_{\alpha}(Q_2)\{\exp[-M_{\alpha}(\mathbf{Q}_1-\mathbf{Q}_2)] - \exp[-M_{\alpha}(Q_1)-M_{\alpha}(Q_2)]\}. \qquad (4)$$

A brief derivation, based on the Hall & Hirsch model, is given in the Appendix. Here $f_{\alpha}(Q)$ is the elastic scattering amplitude for an atom of type α and a scattering vector $\mathbf{Q}$. The Debye–Waller terms are

$$M_{\alpha}(Q) = \tfrac{1}{2}Q^{2}\langle u^{2}_{\alpha}\rangle, \qquad (5)$$

where $\langle u^{2}_{\alpha}\rangle$ is the mean-square displacement along the vector $\mathbf{Q}$. For $\mathbf{Q}_1 = \mathbf{Q}_2$, [kin] reduces to the readily interpretable factor

$$[\text{kin}] = f^{2}(Q)\{1-\exp[-2M(Q)]\} \qquad (6)$$

(see James, 1948). With the X-ray scattering amplitudes of Cromer & Waber (1965) and the Doyle & Turner (1968) parameters for scattered electron amplitudes, this function is plotted in Fig. 1 for titanium. The peak in the Einstein distribution for electrons (here at $q/2\pi = 1/\lambda = 0{\cdot}22$ Å^{-1}) is contrasted with a maximum at $1{\cdot}2$ Å^{-1} for X-rays. Here a typical room-temperature $\langle u^{2}_{\alpha}\rangle$ of $0{\cdot}005$ Å^{2} is assumed. The maxima for oxygen are displaced outwards (towards larger Q) by about 20%.

Equation (1) may be thickness averaged by reducing the branch index summation to one over ij' alone, so that only t-independent terms are considered. This could be regarded as equivalent to an independent Bloch-wave model, which, as shown by Cherns, Howie & Jacobs (1973), differs from the dependent Bloch-wave description for small t. For t greater than the extinction distance, the differences become small and this technique of t averaging is perhaps more reliable. It also has a computational advantage. In general there are NB^{8} terms per pixel to be considered in the calculation, where NB = number of beams included. This reduces to NB^{6} when thickness averaged.

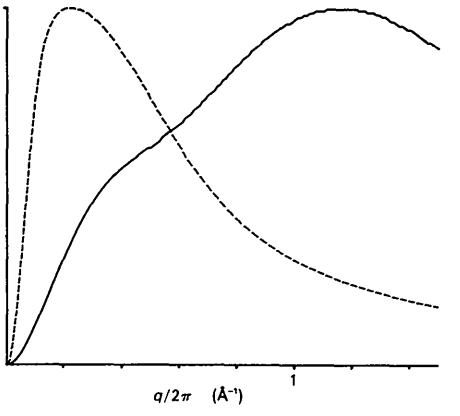

Fig. 1. The TDS intensity for electrons (dashed line) and X-rays (solid line) as a function of scattering vector $q/2\pi = 1/\lambda$ for Ti. Here $\langle u^{2}_{i}\rangle$ is assumed to be 0·005 Å.

For scattering from a Bloch wave to plane wave, and assuming δ-function scattering sources at τ, it has been shown by Rossouw & Maslen (1984) that (1) reduces to the standard expression for current density (apart from the factor nt), *i.e.*

$$J(\mathbf{k}, \tau) = \sum_i |C_0^i|^2 |B^i(\mathbf{k}^i, \tau)|^2. \quad (7)$$

3. Computer simulations

In the following computations for 100 keV electrons, the Bloch-wave matrix was constructed from Doyle–Turner parameters (Doyle & Turner, 1968) for the atomic scattering amplitudes. These were inserted in the tetragonal unit cell for rutile (space group P_4/mnm), with cation coordinates [000], $[\frac{1}{2}\frac{1}{2}\frac{1}{2}]$ and anion coordinates $[uu0]$, $[\bar{u}\bar{u}0]$, $[\frac{1}{2}+u\ \frac{1}{2}-u\ \frac{1}{2}]$ and $[\frac{1}{2}-u\ \frac{1}{2}+u\ \frac{1}{2}]$. Here $a = 4{\cdot}5937$, $c = 2{\cdot}9581$ and $u = 0{\cdot}3053$ Å. The c-axis projection of the rutile structure is given in Fig. 2(a).

In § 3(a), current density calculations are introduced for intuitive interpretation of the diffuse scattering phenomena. § 3(b) presents t-averaged TDS calculations from (1) (NB = 9, symmetrical c-axis projection). Comparison with experiment is made in § 4. Eigenvectors and eigenvalues were calculated from Eispack subroutines (Smith, Boyle, Dongarra, Garbow, Ikebe, Klema & Moler, 1976), and images photographed from a TV display screen with 16 grey levels.

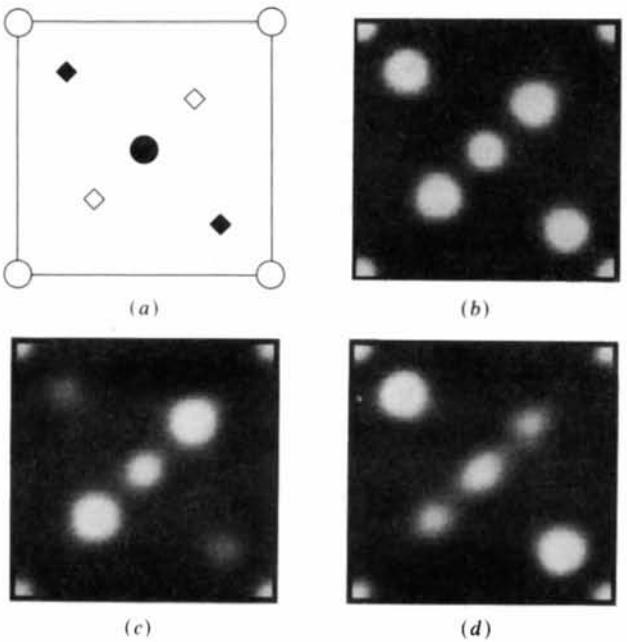

Fig. 2. (a) c-axis projection of the rutile structure, showing cation ○ (● in the plane beneath the paper) and anion ◇ (◆ beneath). (b)-(d) 45-beam calculations for current density in TiO_2, with the minimum value subtracted from the distribution for greater clarity. The orientations are: (b) [0, 0, 0] (max. = 3·7, min. = 0·26); (c) [0·16, 0·16, 0] (max. = 4·85, min. = 0·19); (d) [0·28, 0·28, 0] (max. = 4·46, min. = 0·21). Orientations (c) and (d) are indicated in Fig. 4(b).

(a) *Current density variations*

To understand the angular dependence of the TDS, we need to know how the fast-electron current density in the unit cell changes as a function of $\mathbf{k}' = \mathbf{k} - \mathbf{q}$. If both ψ and ψ' have current densities (J and J') with maxima on a localized inelastic source at τ, an excess loss signal will be generated in the direction $\mathbf{k}'$. However, if J' has a local minimum on τ, decoupling occurs for the $\psi \rightarrow \psi'$ transition, leading to deficient scattering in the direction $\mathbf{k}'$. Figs. 2(b)-(d) show 45-beam c-axis projections of the current density in the rutile unit cell. Following Cowley (1981), we use uvw as coordinate variables in reciprocal space. The distribution changes with crystal tilt as indicated, with orientation $[uvw]$ defined as the vector from the origin [000] to the centre of the Laue circle. As 110 is tilted towards the Ewald sphere, maxima increase on one pair of oxygen sites, and are displaced onto the other pair of oxygen sites with further tilt. Dynamical diffuse structure reflects the orientation dependence of current density on localized scattering sources and, since rapid fluctuations occur on these sites as diffracted beams in ψ' are brought into the exact Bragg orientation, this structure represents an image of the Brillouin zone (BZ) boundaries.

The orientation $[u'v'w']$ for the inelastically scattered beam must be referred to the orientation $[uvw]$ of the elastic beam on the diffraction pattern. For a symmetrical Laue orientation, $[uvw] = 0$, and BZ boundaries bisect the diffracting vectors $\mathbf{g}$. This position indicates where the projection of $\mathbf{k}'$ along $\mathbf{g}$ is $-\frac{1}{2}\mathbf{g}$, so that $\mathbf{g}$ in ψ' is in the exact Bragg orientation. For a point $\mathbf{p}$ in the diffraction pattern, $[u'v'w'] = [uvw] - \mathbf{p}$. Thus the edges of Kikuchi bands in the diffraction pattern are located at the BZ boundaries, reflecting sharp changes of current density in the unit cell. Note that, for quasi-elastic TDS, $\mathbf{p} \simeq -\mathbf{q}$.

Fig. 3(a) is a 13-beam systematic row calculation, with current on Ti and O sites plotted as a function of orientation. In Figs. 3 and 4, the current density associated with ψ on each site is constant at the intercept 0; the current density of ψ' on each site is directly projected onto the diffraction pattern, and varies with orientation $[u'v'w']$. For instance, $\psi \rightarrow \psi'$ coupling is related to the real-space overlap of Fig. 2(b) with Figs. 2(c) or (d) at the scattering sites, depending on the orientation of ψ'. In the one-dimensional projection of Fig. 3, two of the O sites have the same projection symmetry as Ti. The current is therefore shown on the remaining two O sites. Within the first BZ, current decreases on Ti and increases on O, without strong perturbation as the second BZ is entered. Relatively abrupt decreases in current on both Ti and O occur as the 220 and

higher-order beams are swept within the Ewald sphere, with a gradual build-up of current on each site until the next Bragg reflexion intersects the Ewald sphere.

Fig. 3(*b*) shows a 13-beam systematic row calculation along ⟨100⟩. Current density increases on Ti sites as the 200 beam is tilted from its symmetrical orientation towards the Ewald sphere, compared with a decrease on O sites. However, when the 200 reciprocal-lattice point passes through the Ewald sphere, maxima flip from Ti to O, and within the second BZ maxima remain on O sites. Beyond 400, a similar build-up and decrease occurs on both Ti and O as higher-order beams are tilted through exact Bragg orientations.

The angular dependence of the current density of the inelastic beam on the various sites may be plotted as a two-dimensional **q** variation, directly superimposed on a diffraction pattern. Fig. 4 shows a 45-beam calculation, showing the variation on Ti in 4(*a*) and one of the O sites in 4(*b*). The first-order BZ boundaries are schematically illustrated in Fig. 4(*a*). Several BZ's intersect, and sharp variations occur near BZ boundaries. The Ti response varies smoothly across 100 (as the 200 BZ boundary is crossed) and across the 220 BZ boundary. This contrasts with the angular dependence of current density on oxygen, where current density within BZ's varies quite sharply. Fig. 4(*c*) shows the summation of current density on all O sites, where a sharp drop past 110 (the 220 BZ boundary) defines a square with {200} beams as vertices.

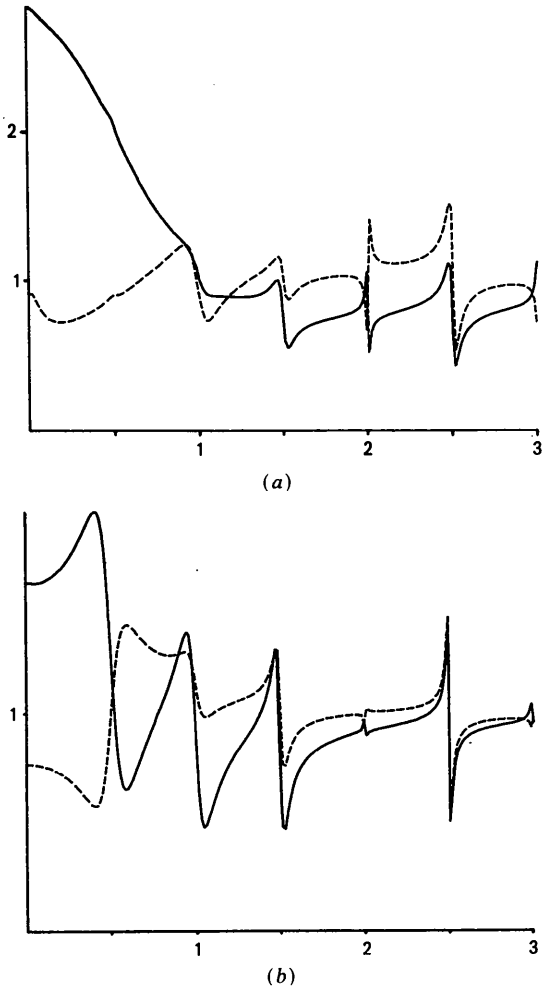

Fig. 3. Current density on Ti (solid line) and O (dashed line) sites with different projection symmetry, as a function of crystal orientation, 13-beam systematic row computations. The x axis indicates the projection of the fast electron wavevector on the reciprocal lattice (this is half the vector from the origin to the intersection of the reciprocal lattice with the Ewald sphere) measured in units of (*a*) ⟨110⟩ and (*b*) ⟨200⟩.

(*b*) *An Einstein TDS computation*

A nine-beam computation for TDS from rutile at room temperature is shown in Fig. 5. Isotropic r.m.s. displacements were assumed to be 0·067 Å for O and 0·075 Å for Ti, as derived from the X-ray data of Abrahams & Bernstein (1971). The computed response from the Ti and O sites show BZ boundary images as for the current density calculations of Fig. 4. However, since the [kin] term has properties very different to a δ-function scattering potential, a radical redistribution of intensity between BZ's is evident. For Ti, pronounced deficit scattering occurs near the centre, and deficit streaks along ⟨110⟩. Deficit lobes are directed inwards from {200} beams. For O, there is some similarity between Figs. 4 and 5(*b*), with a redistribution of intensity in Fig. 5(*b*) towards larger **q**. The summed O-site response in Fig. 5(*c*) shows excess lobes directed inwards from the {200} beams to the origin, caused by the summation of 5(*b*) with a similar pattern rotated by $\pi/2$. The 200 BZ boundary (the square with {110} beams as vertices) is evident, with deficit scattering in the centre. Since only nine beams are considered, structure outside the 200 BZ may be meaningless.

The computed maximum from the two Ti sites is about four times greater than the maximum from all four O sites. This is primarily due to the peaking of current density for the elastic beam on Ti sites when the crystal is in the symmetrical orientation, but also reflects the ratio f_{Ti}/f_O and the somewhat larger r.m.s. displacement for Ti compared with oxygen.

7. Comparison with experiment

Observations of TDS for the [001] projection of rutile have been presented by Bursill & Rossouw (1984). New phenomena included intense diffuse scattering directed inwards from {200} reflexions, a sharply-defined square of continuous intensity having {200} beams as vertices, relatively sharp ⟨110⟩ streaking along radial and non-radial directions, and a distinct

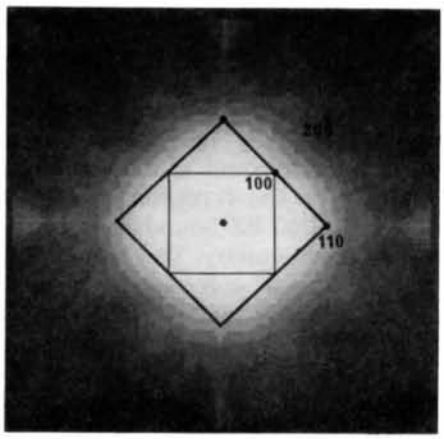

(*a*)

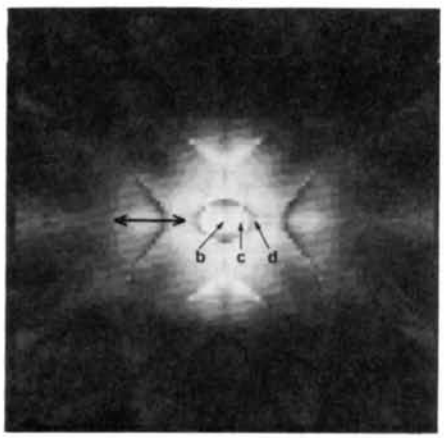

(*b*)

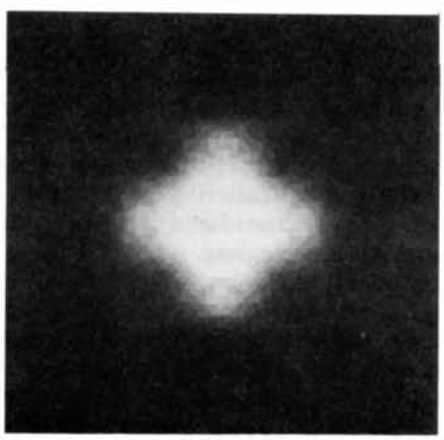

(*c*)

Fig. 4. (*a*) Two-dimensional plot of current density on Ti sites, superimposed on a diffraction pattern (max. 3·66, min. 0·46). Here and in all other 2D maps, the minimum value is subtracted so that the distribution is enhanced. The fine line indicates the area enclosed by 110 BZ's and the thick line indicates the 200 BZ boundaries. Positions of 100, 110 and 200 beams are indicated. (*b*) Similar plot of current density on O sites with the same projection symmetry (max. 5·53, min. 0·34), the direction of nearest-neighbour Ti atoms is indicated by the heavy double-arrowed marker. The orientations chosen for plots of current density in Figs. 2(*b*)-(*d*) are indicated. (*c*) Current density on all O sites (max. 3·8, min. 0·45), a summation of (*b*) with an equivalent distribution rotated by $\pi/2$.

deficit scattering region surrounding the transmitted beam (*cf.* Fig. 6). Both the angular dependence of the TDS with respect to crystal tilts and the temperature variation of TDS in the range $90 < T < 420$ K were also described.

As shown above, diffuse streaking and areas of excess diffuse scattering have their origin in the vari-

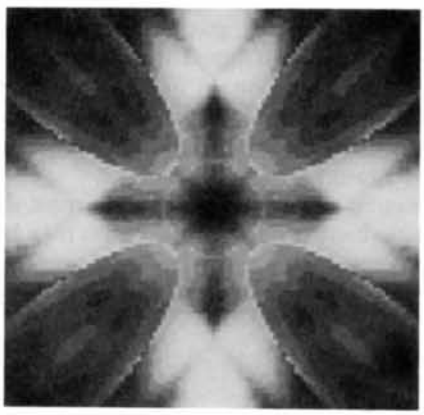

(*a*)

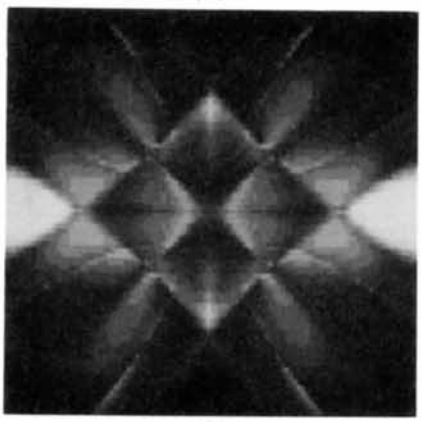

(*b*)

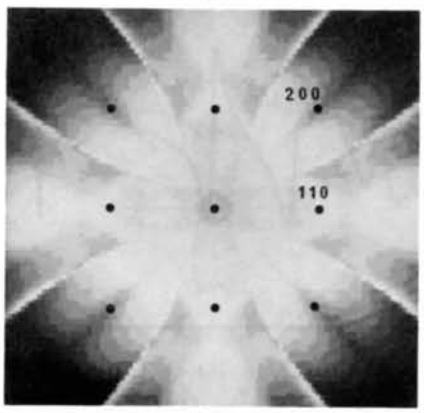

(*c*)

Fig. 5. (*a*) Nine-beam map of TDS from Ti sites (max. 0·33, min. 0·014). (*b*) TDS from two O sites with the same projection symmetry (max. 0·05, min. 0·014). (*c*) Summation of TDS from all O sites (max. 0·071, min. 0·028), with a superimposed diffraction pattern.

ations in current density within the unit cell, taking into account the site(s) τ and scattering vector $\mathbf{q}$. The features brought out most clearly in the calculations are visible in the experimental patterns, *i.e.* streaking in ⟨110⟩ directions out of the 000 beam (point scattering model equivalent to current density), and diffuse maxima, minima and lobes (Einstein model). Theoretical predictions should improve when more Bragg beams can be included although, at present, this is limited by available computing resources.

Note that dynamical effects couple to crystal orientation, *i.e.* Kikuchi bands will move across the diffraction pattern as the crystal is tilted. Experiment confirms that slight misorientations from the c axis destroy the symmetry of these diffuse patterns (see Fig. 3 of Bursill & Rossouw, 1984). Streaking due to phonon modes is not in this sense a dynamical phenomenon, since these will not be displaced on the diffraction pattern with crystal tilt.

The c-axis diffraction pattern from TiO_2 in Fig. 6 (Bursill & Rossouw, 1984) show diffuse streaks in ⟨110⟩ directions from the (000) beam, and an intense diffuse square connecting the {200} beams. This square seems most closely related to the current density variations on O sites (Fig. 5c), and streaking in ⟨110⟩ directions is supported in both Figs. 4(c) and 5(c). Broad lobes pointing inwards from the {200} beams are also simulated in the TDS from O sites in Fig. 5(c). If the total computed TDS from O plus Ti is displayed, the distribution is not much different from Fig. 5(a), and correlation with experiment is disappointing. However, correlation between experiment and the expected response from O sites may be significant.

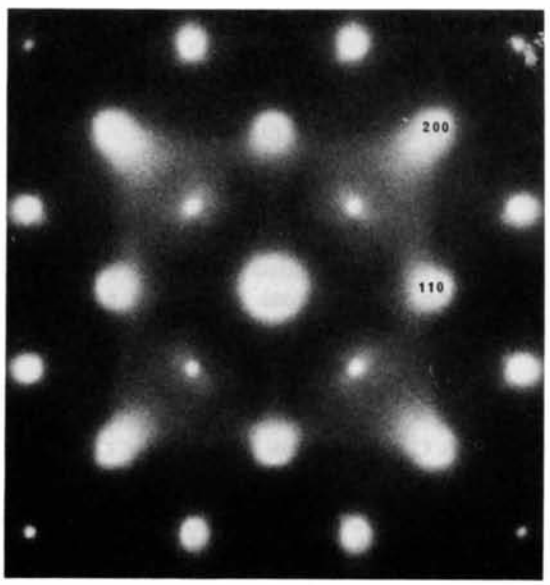

Fig. 6. Experimental c-axis diffraction pattern from TiO_2. Here some intensity from forbidden {100} diffracted beams occurs. Similarities are evident between this and features in the oxygen-site scattering simulations in Figs. 4(c) and 5(c).

Why oxygen sites should apparently contribute far more strongly to diffuse scattering than Ti sites is not well understood. A possible explanation is that the Ti atoms vibrate effectively 'in phase' rather than 'at random' as assumed in the Einstein model, at least for lateral extents of about the same dimensions as the lateral coherence length of the scattered electrons. Thus the Ti sublattice would appear effectively square (and stationary) with respect to fast electrons. It has been reported that, for TiO_2, the (incipient) ferroelectric mode A_{2u} accounts for 20% of the vibrational energy at 300 K (Samara & Peercy, 1973). The atomic displacements for this mode lie strictly parallel to [001] (the projection axis used in the present study, see Fig. 14, Bursill, 1978/79). Clearly, to proceed further in the analysis of TDS from rutile-type structures, more elaborate and realistic modelling of the vibrational modes must now be contemplated.

8. Conclusion

The theory presented in this paper extends the two-beam theory of Hall & Hirsch (1965), and provides an Einstein model for TDS that is valid for all scattering angles. Theories involving phonon scattering (Rez, Humphreys & Whelan, 1977; Earney, 1971) are usually approximated to first order, so that the theory breaks down at large angles where multiple phonon processes contribute to TDS.

New diffuse scattering phenomena in rutile structures have at least been partially explained in terms of point scattering and an Einstein TDS model. Simple arguments based on current densities associated with elastic and inelastic wavefunctions, and how these affect coupling between these states, may also provide an intuitive understanding of dynamical diffuse scattering phenomena. At this stage more detailed scattering models suffer from limited resolution because of severe computational restrictions on the number of beams.

Nevertheless, it is already clear that the present theoretical calculations have provided a significant first step towards the quantitative analysis of TDS for electrons. This theory may be extended to cover X-ray or neutron scattering. Further experimental studies, in particular measurement of the temperature dependence of the diffuse scattering from TiO_2, MgF_2 and other isostructural compounds, are in progress.

We are grateful to Russel Creek, Peter Goodman, Sylvia Mair, Peter Self and Alan Spargo for stimulating discussions and to Denis Lynch for assistance with the computations. We acknowledge the financial support of a CSIRO/University of Melbourne research grant.

APPENDIX

We follow Hall & Hirsch (1965), but extend their treatment by writing both elastic and inelastic wavefunctions as Bloch waves, *i.e.*

$$\psi = \sum_j A^j \sum_h C_h^j \exp\{i(\mathbf{k}^j + \mathbf{h}) \cdot \mathbf{r}\}$$

and (A1)

$$\psi' = \sum_{j'} A^{j'} \sum_{g'} C_{g'}^{j'} \exp\{i(\mathbf{k}^{j'} - \mathbf{g}') \cdot \mathbf{r}\}.$$

The crystal atoms α, β vibrate as Einstein oscillators, with instantaneous positions

$$\mathbf{r}'_\alpha = \mathbf{r}_\alpha + \mathbf{u}_\alpha \qquad (A2)$$

with $\mathbf{u}_\alpha$ the thermal displacement from equilibrium $\mathbf{r}_\alpha$. The scattered amplitude Y, including both Bragg and TDS contributions, is thus

$$Y = \sum_\alpha \psi'^*(\mathbf{r}'_\alpha) f_\alpha(\mathbf{Q}_1) \psi(\mathbf{r}'_\alpha), \qquad (A3)$$

where f is the atomic scattering amplitude, and $\mathbf{Q}_1 = \mathbf{q} + \mathbf{h} - \mathbf{g}'$ connects discrete beams in ψ and ψ' to a position $\mathbf{q}$ in reciprocal space. Writing the total intensity I_T as YY^*, and substituting (A1) into (A3), we have

$$I_T = \mathrm{SUM} \sum_{\alpha,\beta} f_\alpha(Q_1) f_\beta^*(Q_2) \times \exp\{iQ_1 \cdot \mathbf{r}'_\alpha\} \exp\{-i\mathbf{Q}_2 \cdot \mathbf{r}'_\beta\}. \qquad (A4)$$

Here $\mathbf{Q}_2 = \mathbf{q} + \mathbf{g} - \mathbf{h}'$ and

$$\mathrm{SUM} = \sum_{index} A^{i*} A^j A^{i'*} A^{j'} C_g^{i*} C_h^j C_{g'}^{i'*} C_{h'}^{j'}$$

with the sum over *index* including branch indices i, j, i', j' and beams g, h, g', h'.

We split the sum over atoms α, β in (A4) into a sum over $\alpha = \beta$ and $\alpha \neq \beta$. Thus

$$T_1 = \sum_\alpha f_\alpha(Q_1) f_\alpha^*(Q_2) \exp\{i(\mathbf{Q}_1 - \mathbf{Q}_2) \cdot \mathbf{r}'_\alpha\}$$

$$T_2 = \sum_{\alpha \neq \beta} f_\alpha(Q_1) f_\beta^*(Q_2) \exp\{i(\mathbf{Q}_1 \cdot \mathbf{r}'_\alpha - \mathbf{Q}_2 \cdot \mathbf{r}'_\beta)\}.$$

Using (A2) and the relationship $\langle \exp\{i\mathbf{Q} \cdot \mathbf{u}\} \rangle = \exp\{-\frac{1}{2}\langle(\mathbf{Q} \cdot \mathbf{u})^2\rangle\}$, the thermal average of the first term is

$$T_1 = \sum_\alpha f_\alpha(Q_1) f_\alpha^*(Q_2) \exp\{i(\mathbf{Q}_1 - \mathbf{Q}_2) \cdot \mathbf{r}_\alpha\} \times \exp\{-M(\mathbf{Q}_1 - \mathbf{Q}_2)\}. \qquad (A5)$$

Likewise, the thermal average of the second term is

$$T_2 = \sum_{\alpha \neq \beta} f_\alpha(Q_1) f_\beta^*(Q_2) \exp\{i(\mathbf{Q}_1 \cdot \mathbf{r}_\alpha - \mathbf{Q}_2 \cdot \mathbf{r}_\beta)\} \times \exp\{-[M(Q_1) + M(Q_2)]\}. \qquad (A6)$$

The total intensity is then

$$I_T = I_B + I_{\mathrm{TDS}} = \mathrm{SUM}[T_1 + T_2]. \qquad (A7)$$

The Bragg contribution is obtained by writing the intensity from α, β at equilibrium positions, but with $f(Q)$ modulated by the Debye-Waller factor $\exp\{-M(Q)\}$. Using similar arguments to those in obtaining (A7), we find

$$I_B = \mathrm{SUM}[W_1 + W_2], \qquad (A8)$$

where

$$W_1 = \sum_\alpha f_\alpha(Q_1) f_\alpha^*(Q_2) \exp\{i(\mathbf{Q}_1 - \mathbf{Q}_2) \cdot \mathbf{r}_\alpha\} \times \exp\{-[M(Q_1) + M(Q_2)]\}$$

and $W_2 = T_2$. Thus

$$I_{\mathrm{TDS}} = I_T - I_B = \mathrm{SUM}[T_1 - W_1], \qquad (A9)$$

where the sum over products $\alpha \neq \beta$ cancel out, leaving only self-correlated terms in (A9). The term in square brackets in (A9), *i.e.*

$$\sum_\alpha f_\alpha(Q_1) f_\alpha^*(Q_2) \exp\{i(\mathbf{Q}_1 - \mathbf{Q}_2) \cdot \mathbf{r}_\alpha\} \times (\exp[-M(\mathbf{Q}_1 - \mathbf{Q}_2)] - \exp\{-[M(Q_1) + M(Q_2)]\}) \qquad (A10)$$

is equivalent to the combined term [site] [kin] in (3) and (4), summed over all atoms α. Thus we have the [kin] term as a function of 'non-aligned' terms in $\mathbf{Q}_1$ and $\mathbf{Q}_2$. The above treatment is readily extended to include crystals with m atoms of type α per unit cell. A more convenient expression, which requires a sum over atoms in the unit cell, is written

$$I_{\mathrm{TDS}} = nt \sum_{index} [\mathrm{site}][\mathrm{kin}][k, k'], \qquad (A11)$$

where, from (A10),

$$[\mathrm{site}] = \sum_{\alpha m} \exp\{i(\mathbf{Q}_1 - \mathbf{Q}_2) \cdot \boldsymbol{\tau}_{\alpha m}\} \qquad (A12)$$

$$[\mathrm{kin}] = f_\alpha(Q_1) f_\alpha^*(Q_2) \times (\exp\{-M(\mathbf{Q}_1 - \mathbf{Q}_2)\} - \exp\{-[M(\mathbf{Q}_1) + M(\mathbf{Q}_2)]\}) \qquad (A13)$$

and $[k, k']$ as in (4). It is also possible to derive (A13) by inspection of the cross term in $\mathbf{q}$ and $\mathbf{q} - \mathbf{g}$ in equation (10) of Hall & Hirsch (1965).

References

ABRAHAMS, S. C. & BERNSTEIN, J. L. (1971). *J. Chem. Phys.* **55**, 3206-3211.

BURSILL, L. A. (1978/79). *Chem. Scr.* **14**, 83-97.

BURSILL, L. A. & ROSSOUW, C. J. (1984). *J. Microsc.* **136**, 153-164.

CHERNS, D., HOWIE, A. & JACOBS, M. H. (1973). *Z. Naturforsch. Teil A*, **28**, 565-571.

COWLEY, J. M. (1981). *Diffraction Physics*, 2nd ed. p. 91. New York: North-Holland.

CROMER, D. T. & WABER, J. T. (1965). *Acta Cryst.* **18**, 104-109.

DOYLE, P. A. & TURNER, P. S. (1968). *Acta Cryst.* A**24**, 390-397.

EARNEY, J. J. (1971). *Philos. Mag.* **23**, 577-583.

HALL, C. R. & HIRSCH, P. B. (1965). *Proc. R. Soc. London Ser. A*, **286**, 158-177.
HOWIE, A. (1963). *Proc. R. Soc. London Ser. A*, **271**, 268-287.
HUMPHREYS, C. J. (1979). *Rep. Prog. Phys.* **42**, 1825-1887.
JAMES, R. W. (1948). *The Optical Principles of the Diffraction of X-rays*, p. 259. London: Bell.
MASLEN, V. W. & ROSSOUW, C. J. (1984). *Philos. Mag.* **49**, 735-742.
REZ, P., HUMPHREYS, C. J. & WHELAN, M. J. (1977). *Philos. Mag.* **35**, 81-96.
ROSSOUW, C. J. & MASLEN, V. W. (1984). *Philos. Mag.* **49**, 743-757.
SAMARA, G. A. & PEERCY, P. S. (1973). *Phys. Rev. B*, **7**, 1131-1148.
SMITH, B. T., BOYLE, J. M., DONGARRA, J. J., GARBOW, B. S., IKEBE, Y., KLEMA, V. C. & MOLER, C. B. (1976). *Matrix Eigensystem Routines—EISPACK Guide. Lecture Notes in Computer Science*, Vol. 6, edited by G. GOOS & J. HARTMANIS, pp. 19-33. Berlin: Springer-Verlag.
YOSHIOKA, H. (1957). *J. Phys. Soc. Jpn*, **12**, 618-628.

Acta Cryst. (1985). A**41**, 327-333

Program Construction for Macromolecule Atomic Model Refinement Based on the Fast Fourier Transform and Fast Differentiation Algorithms

BY V. YU. LUNIN AND A. G. URZHUMTSEV

Research Computer Center, USSR Academy of Sciences, 142292 *Pushchino, Moscow Region, USSR*

(*Received* 9 *November* 1983; *accepted* 13 *December* 1984)

Abstract

Structure refinement may be considered as a minimization of a function $R(\chi)$ of a large number of refineable parameters. A new type of function incorporating phase probability distribution is proposed. The minimization of the function utilizing gradient methods requires the computation of gradient ∇R, as well as the product of the gradient and the matrix of second derivatives with some direction. The algorithm of Kim, Nesterov & Cherkassky [*Dokl. Akad. Nauk SSSR* (1984), **275**, 1306-1309] adapted to macromolecular structure refinement takes about four times longer for the computation of these values compared to the computation of the value of the minimized function. The matrix of second derivatives is used without any approximation.

Introduction

The refinement of a structure implies that there is a model with parameters to be changed until they most closely fit X-ray scattering data, stereochemical restraints, energy minimum conditions *etc.* The refinement proper should be distinguished from the elaboration of its instrumental part, that is computer programs. And if for the former the most important are the researcher's experience and intuition, the latter puts more emphasis on the 'computer' problems such as efficiency of the algorithms, user's convenience *etc.* Different approaches to refinement of macromolecular structures have computational similarities, so that it becomes possible to solve most general problems of developing the corresponding programs.

The large number of refineable parameters is an essential feature of macromolecular structure refinement. This involves considerable computational difficulties, therefore routinely applicable algorithms need computation increasing linearly with the size of the refineable object. The Cooley-Tukey (1965) algorithm based on the fast Fourier transform and the fast differentiation algorithm developed by Kim, Nesterov & Cherkassky (1984) allow a general algorithm for model refinement whose computation per cycle increases almost linearly with the size of molecule. In § 2 we consider the algorithm constructed by Kim *et al.*, in which the n components of the gradient of a function $f(x_1, \ldots, x_n)$ require much the same computation as the single function. Note that an algorithm of this type for some particular criterion used in refinement of atomic models was earlier proposed by Agarwal (1978) and later improved by Lifshitz (Agarwal, 1981). In § 3 we show how to develop similar algorithms for every criterion and refineable parameter. It should be emphasized that these rapid algorithms compute the accurate product of a full second-derivative matrix and a direction without any approximation. Application of the routine based on these algorithms will be considered elsewhere.

1. Problem of the atomic model refinement

1.1. *Atomic models*

In this paper we consider only the models where the distribution of electron density can be a sum of the contributions of individual atoms

$$\rho(\mathbf{r}) = \sum \rho_j(\mathbf{r}, \mathbf{q}_j). \qquad (1)$$

0108-7673/85/040327-07$01.50